J Electr Eng Technol.2015;10(1): 251-260
http://dx.doi.org/10.5370/JEET.2015.10.1.251

ISSN(Print) 1975-0102
ISSN(Online) 2093-7423

A Novel Space Vector modulation Scheme and Direct Torque Control for Four-switch BLDCM Using Flux Observer

Lei Pan†, Beibei Wang*, Gang Su*, Baohua Cheng* and Guili Peng*

Abstract – The main purpose of this paper is to describe a DTC (direct torque control) method for four-switch brushless dc motor (BLDCM) drive. In the method, a novel voltage space vector modulation scheme, an optimal switching table, and a flux observation method are proposed. Eight voltage vectors are summarized, which are selected to control BLDCM in SVPWM pattern, and an optimal switching table is proposed to improve the torque distortion caused by midpoint current of the split capacitors. Unlike conventional flux observers, this observer does not require speed adaptation and is not susceptible to speed estimation errors, especially, at low speed. Global asymptotic stability of the flux observer is guaranteed by the Lyapunov stability analysis. DC-offset effects are mitigated by introducing a PI component in the observer gains. This method alleviates the undesired current and torque distortion which is caused by uncontrollable phase. The correctness and feasibility of the method are proved by simulation and experimental results.

Keywords: Four-switch inverter, Voltage space vector, Flux observer, BLDCM, Optimal switching table

1. Introduction

As BLDCMs have such good features as simple construction, high reliability, light electromagnetic pollution, and high power density, they are used extensively in servo systems and low-power drive systems [1, 2].

FSTPI (four-switch three phase inverter) as a reconfiguration topology for fault condition of traditional six switch inverter has been widely used [3-5]. But the uncontrollable phase current causes unsymmetrical voltage vector in FSTPI, and its waveform is much of distortion from rectangular [3]. A new speed control method using the acceleration feed forward compensation is proposed to improve the speed response characteristic for a four-switch three-phase BLDCM [4]. The disturbance torque estimation method is adopted to improve the robustness of the method. But it is just verified to be economical and efficient in some occasions with light load, such as robot arm. A study on the generated torque ripples due to phase commutation is presented in the four-switch three-phase BLDCM [6], in which a current control technique is developed to minimize commutation torque for the entire speed range. But Hall sensor is used in this method and the cost of the system is raised. A novel direct torque control scheme [7] including the actual pre-stored back-EMF constants vs. electrical rotor position look-up table is proposed for BLDCM drive with two phase conduction scheme using four-switch inverter. And low-frequency torque ripples and torque response time are minimized. But the control method is more complicated, and does not discuss flux change characteristics.

In this paper, a novel voltage space vector modulation strategy and an optimal switching table are proposed to provide a basic condition for improve torque control. A single neuron adaptive PID method is proposed to observe flux for providing the accurate control information. The operating principle of FSTPI for the three-phase BLDCM drive and the proposed control scheme are explained. The validity of the proposed system is verified by simulation and experimental results.

2. Phase Current Analysis of Traditional Four Switching Patterns

The FSTPI topology consists of 4 power switches that provide two of the inverter output phases. The third phase is fed by the dc link from the center of a split-capacitor, as shown in Fig. 1.

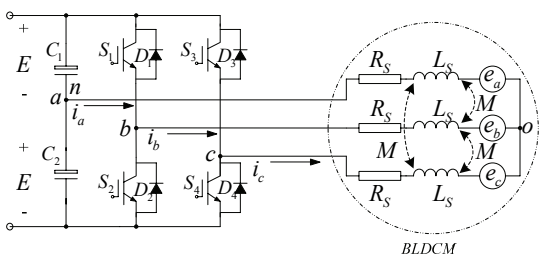

Fig. 1. Power Circuit of FSTPI

† Corresponding School of Control and Mechanical Engineering, Tianjin Chengjian University, Tianjin, China. (panlei4089@163.com)
* School of Control and Mechanical Engineering, Tianjin Chengjian University, Tianjin, China. ({wbbking, sgltu, 297684750}@qq.com, planepeople678@sina.com)
Received: March 7, 2013; Accepted: September 24, 2014

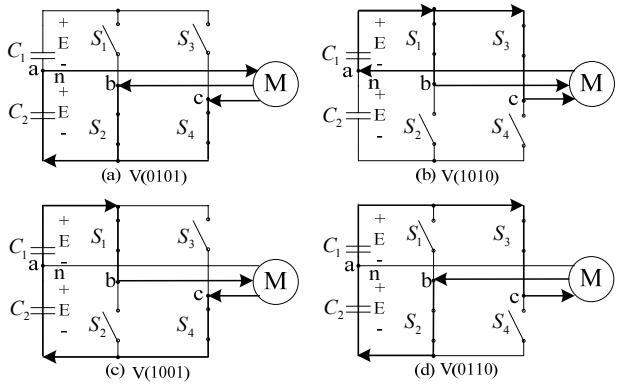

Fig. 2. Conventional four-switch voltage vector topology

In FSTPI system, there are four possible switching patterns to generate three-phase currents, as shown in Fig. 2 with ideal switches; these four switching patterns are V(0101), V(1010), V(1001), and V(0110), where "0" means the switch is turned off and "1" the switch is turned on in inverter. In the same figure, the free- wheeling diodes are ignored. In six-switch inverter, two zero voltage space vectors cannot supply the dc-link to the load, therefore no current flows through the load. The main difference of the four-switch inverter compared to its counterpart six-switch one is that one phase is always connected to the center tap of the split capacitors, so that there will always be current flowing through that phase even with voltage vectors V(0101) and V(1010), as shown in Fig. 2. Under balanced load condition with four-switch topology, there will be no current flow through the phase which is connected to the midpoint of the split capacitors using two possible non-zero voltage vectors, V(1001) and V(0110), as shown in Fig. 2. When voltage vectors V(1001) and V(0110) are used and the load is not completely balanced, only the resultant current of the other two phases flow through the phase connected to the midpoint of the split capacitors. This phenomenon will cause the ripple of current and torque. The simulation curves of current under 15rpm and 5Nm load using four-switching pattern is shown in Fig. 3.

In addition, three different cases may be found at the commutation moment:

Case A: decaying current (i_d) vanishes at the same time rising current (i_r) reaches to its final value +I in Fig. 4(a).

Case B: decaying current (i_d) vanishes before rising current (i_r) reaches to it final value +I in Fig. 4(b).

Case C: rising current (i_r) reaches the value +I before decaying current (i_d) vanishes in Fig. 4(c).

In case B and case C, current disturbance flowing through the phase connected to the midpoint of the split capacitors will cause distortion of magnetic linkage and pulsation of torque.

To solve above problems, this paper proposed a novel space vector modulation method and an optimal switching table.

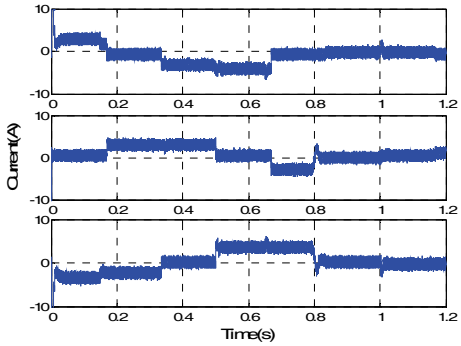

Fig. 3. Current curves using four-switching pattern

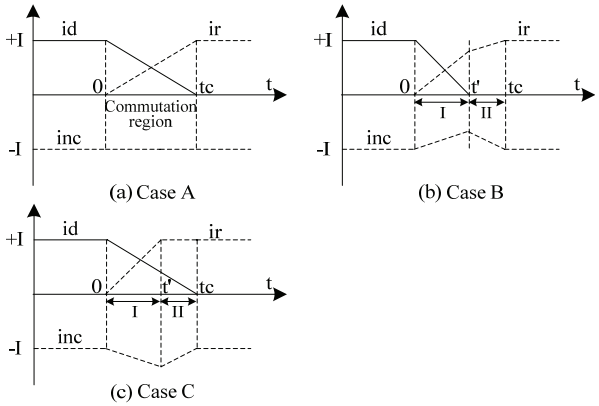

Fig. 4. Current behaviors during commutation

3. DTC of BLDCM Using FSTPI

The typical mathematical model of a three-phase BLDCM is described as:

$$\begin{bmatrix} v_{ao} \\ v_{bo} \\ v_{co} \end{bmatrix} = \begin{bmatrix} R_s & 0 & 0 \\ 0 & R_s & 0 \\ 0 & 0 & R_s \end{bmatrix} \begin{bmatrix} i_a \\ i_b \\ i_c \end{bmatrix} + \frac{d}{dt} \begin{bmatrix} L_s & 0 & 0 \\ 0 & L_s & 0 \\ 0 & 0 & L_s \end{bmatrix} \begin{bmatrix} i_a \\ i_b \\ i_c \end{bmatrix} + \begin{bmatrix} e_{ao} \\ e_{bo} \\ e_{co} \end{bmatrix} \quad (1)$$

$$\begin{cases} v_{ao} = v_{an} + v_{no} = v_{no} \\ v_{bo} = v_{bn} + v_{no} \\ v_{co} = v_{bn} + v_{no} \end{cases} \quad (2)$$

Where, v_{ao} , v_{bo} , and v_{co} are phase voltages; R_s is stator resistance; L_s is stator inductance ; i_a, i_b, and i_c are phase currents; e_{ao}, e_{bo}, and e_{co} are phase back-EMFs.

3.1. Novel space vector modulation method

Generating a 120 electrical degree current conduction is inherently difficult with the conventional four-switch topology, because a BLDCM with non-sinusoidal back-EMF (i.e. trapezoidal) requires a quasi-square wave current profile to generate constant output torque compared to that of a permanent magnet synchronous motor with sinusoidal back-EMF requiring sinewave current. These currents which have 120 electrical degrees conduction period are synchronized with the flat portion of the corresponding

Table 1. The controlling voltage space vector and switch combination

	V_{ao}	V_{bo}	V_{co}	$S_1S_2S_3S_4$ (1:on; 0:off)
V_0	2/3E	-1/3E	-1/3E	0101
V_1	1/2E	0	-1/2E	0001
V_2	0	E	-E	1001
V_3	-1/2E	1/2E	0	1000
V_4	-1/2E	0	1/2E	0010
V_5	0	-E	E	0110
V_6	1/2E	-1/2E	0	0100
V_7	-2/3E	1/3E	1/3E	1010

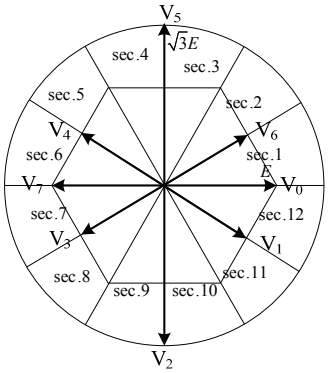

Fig. 5. Voltage space vector chart ($V_x=V_{ao}+V_{bo}+V_{co}$, x= 0,1,2,3,4,5,6,7)

phase back-EMFs, therefore a smooth electromagnetic torque can be obtained. As a result, at every instant of time only two phases conduct and the other phase is supposed to be inactive.

Although four voltage vectors in conventional four-switch inverter system are sufficient enough to control the three-phase ac motors using PWM techniques, it will cause the ripple of current in BLDCM drive, which is shown in Fig. 3. So, additional voltage vectors are required for BLDCM with two phase conduction mode in order to control the midpoint current of the split capacitors at a desired value [8, 9]. Since the conventional method cannot provide a two- phase conduction method completely, a new modulation scheme with new switching patterns should be developed such that only two of the three motor phases conduct.

To obtain the switch modes of operation in four-switch BLDCM drive, a novel voltage vector selection look-up table is designed as shown in Table 1 and the Table 1 is concluded by the four-switch voltage vector topology which is shown in Fig. 6. Based on the Table 1, implementation of the voltage space vectors is depicted in Fig. 5.

3.2. Optimal switching table

Traditional DCC (direct current control) technique employs current hysteresis control [3, 10]. Normally, six-possible voltage space vectors of four-switch topology are supposed to be used in Table 2 as shown in Figs. 6(a)-(f)

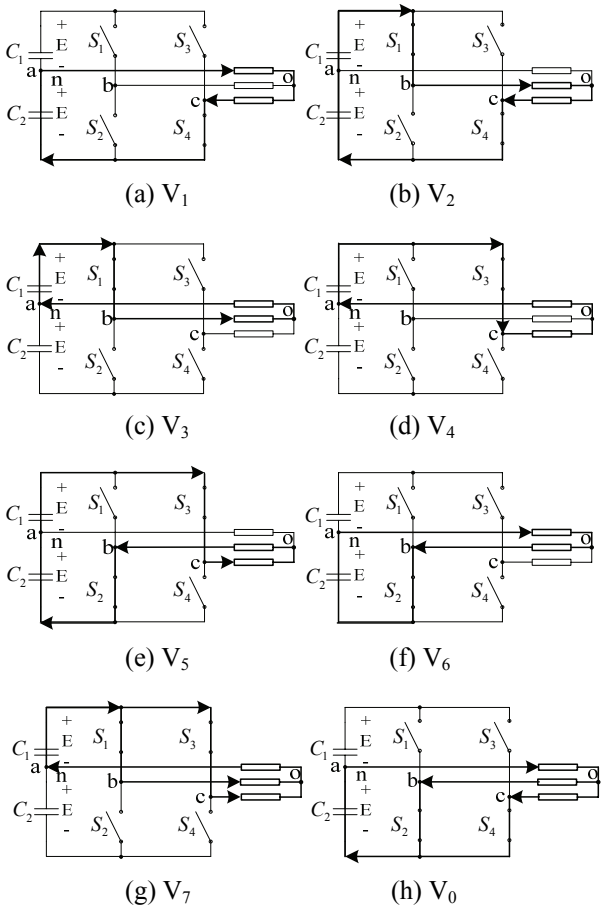

Fig. 6. Four-switch voltage vector topology

similar to the six-switch version, however two of the voltage vectors V2 and V5 as shown in Fig. 6 create problems in the current control. When they are directly used in the voltage vector selection table (Table 2), back-EMF of the uncontrolled phase (phase-a) generates undesired current and distortions occur in each phase current. As a result, undesired electromagnetic torque is inevitable. Therefore, when the rotor position is in the sec.1, 2, 4, 5, 7, 8, 10 and 11, special switching pattern should be adapted.

Additional two voltage vectors V_0 and V_7 which are unused in conventional four-switch PWM scheme are included in the optimal switching table to obtain torque in two-phase conduction four-switch BLDCM drive. The reason is there will be always current trying to flow in phase *–a* due to its back-EMF and the absence of switches controlling its current. As a result, there will be a distorted current in phase*–a* as well as in phase*–b* and *–c*. Therefore, voltage space vectors of phase*–b* and *–c* conduction can be difficult to implement for BLDCM drive unless some modifications are applied to overcome the back-EMF effect of the phase *– a* in these conditions. Selecting the right switching pattern to control the current on phase*–b* and *– c* independently will reduce the distorted currents on those phases and result in a smoother overall current and

Table 2. Four-Switch voltage space vector selection for BLDCM drive

τ_i	sec.1	sec.2	sec.3	sec.4	sec.5	sec.6	sec.7	sec.8	sec.9	sec.10	sec.11	sec.12
1	V5	V5	V4	V4	V3	V3	V2	V2	V1	V1	V6	V6
0	V1	V6	V6	V5	V5	V4	V4	V3	V3	V2	V2	V1

Table 3. Voltage vector selection in sectors II and V for four-switch BLDCM drive (CCW)

τ_T	τ_λ	sec.1	sec.2	sec.3	sec.4	sec.5	sec.6	sec.7	sec.8	sec.9	sec.10	sec.11	sec.12
1	1	V6	V5	V5	V4	V4	V7	V3	V2	V2	V1	V1	V0
	0	V7	V3	V3	V2	V2	V1	V0	V6	V6	V5	V5	V4
0	1	V0	V6	V6	V5	V5	V4	V7	V3	V3	V2	V1	V1
	0	V3	V2	V2	V1	V1	V0	V6	V5	V5	V4	V4	V7

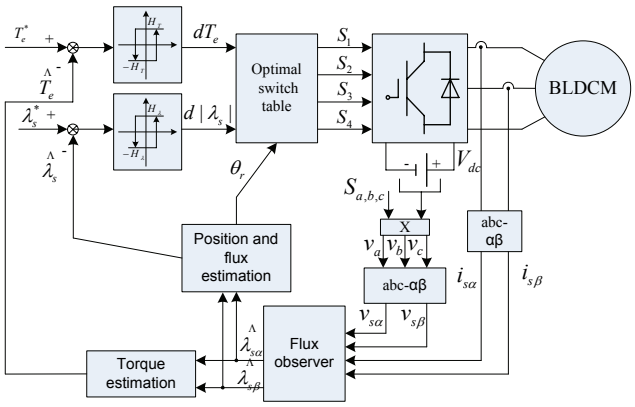

Fig. 7. Schematic of BLDCM control system

electromagnetic torque.

In order to improve the above problems, a DTC method has been proposed as shown in Fig. 7 and explained in detail below:

The DTC method controls instantaneous torque and flux to achieve high-performance operation [11-13]. For this purpose, an optimized switching table must be defined based on the output states of the instantaneous stator flux magnitude hysteresis controller and the electromagnetic torque hysteresis controller, together with the equivalent sector, in which instantaneous stator flux space vector is located [14, 15]. The outputs of hysteresis controller for torque and flux are shown in (3) and (4).

$$\tau_\lambda = \begin{cases} 1, & for \ |\lambda_s^*| - |\lambda_s| > \Delta\lambda_s / 2 \\ 0, & for \ |\lambda_s^*| - |\lambda_s| < \Delta\lambda_s / 2 \end{cases} \quad (3)$$

$$\tau_T = \begin{cases} 1, & for \ T_e^* - T_e > \Delta T_e / 2 \\ 0, & for \ T_e^* - T_e < \Delta T_e / 2 \end{cases} \quad (4)$$

where $\Delta\lambda_s$ is the stator flux hysteresis bandwidth and ΔT_e is the torque hysteresis bandwidth. Since there are eight available switching states in FSTPI, stator flux ($\alpha\beta$) plane is divided into twelve different sectors spaced by 30 electrical degrees and an optimized lookup table (see Table 3) is used to translate these two control states, together with the stator flux position information defined in equivalent sector, to the inverter gate drive signals [16, 17].

In the following, how to eliminate flux disturbance and torque pulsation is explained, when rotor position is in sec. 2 and in CCW direction.

Case A($\tau_T = \tau_\lambda = 1$): in this case, $T_e^* - T_e > \Delta T_e / 2$ and $|\lambda_s^*| - |\lambda_s| > \Delta\lambda_s / 2$, it should increase flux and torque, and V_5 is selected.

Case B($\tau_T = 1$ and $\tau_\lambda = 0$): in this case, $T_e^* - T_e > \Delta T_e / 2$ and $|\lambda_s^*| - |\lambda_s| < \Delta\lambda_s / 2$, it should increase torque and decrease flux, and V_3 is selected.

Case C($\tau_T = 0$ and $\tau_\lambda = 1$): this case is in contrast to the case B, and it should select V_6.

Case D($\tau_T = 0$ and $\tau_\lambda = 0$): this case is in contrast to the case A, and it should select V_2.

In the same way, it can be analyzed, when rotor position in other sectors.

In addition, the direction of the rotor is important to define the specific switching pattern. If the rotor direction is CW, then the above claims are reversed.

This technique has the advantage of not requiring an integration step in the estimation calculation, thus removing problems associated with drift and integral windup [18, 19]. However, it does not rely on the motor parameters and an expensive position sensor.

In the next section, stator flux observation using single neuron adaptive PID is proposed and the observation principle will be analyzed in detail.

4. Flux Calculation

In the $\alpha\beta$ reference frame, the model of flux can be described as:

$$d\lambda_s / dt = u_s - R_s i_s \quad (5)$$

where $\lambda_s = [\lambda_{s\alpha} \ \lambda_{s\beta}]^T$ is the stator flux matrix.

The flux errors are given by:

$$e_\lambda(t) = \lambda_s - \hat{\lambda}_s = \int (v_s - R_s i_s) dt - \hat{\lambda}_s \quad (6)$$

Where $e_\lambda = [\, e_{\lambda\alpha} e_{\lambda\beta} \,]^T$ is the stator flux error matrix, $\hat{}$ denotes the estimated quantities, $v_s = [v_{s\alpha} \ v_{s\beta}]^T$ is the stator

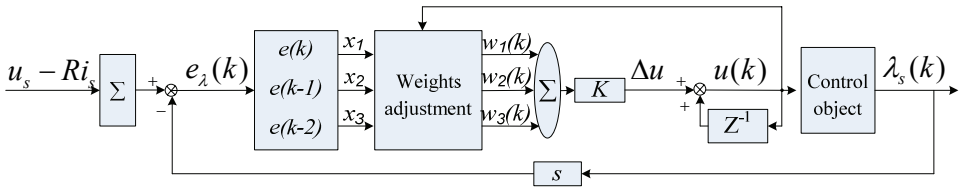

Fig. 8. Schematic of observer of λ_s

voltage matrix, $i_s = [i_{s\alpha}\, i_{s\beta}]^T$ is the stator current matrix.

Based on (6), flux observer is build using single neuron adaptive PID in Fig. 8.

In Fig. 8, the meaning of each part is explained as follows:

After discretization of (6), the input of single neuron adaptive PID is

$$\begin{cases} x_1(k) = e(k) = e_\lambda(k) \\ x_2(k) = \Delta e(k) = e(k) - e(k-1) \\ x_3(k) = \Delta^2 e(k) = e(k) - 2e(k-1) + e(k-2) \end{cases} \tag{7}$$

Assuming the Quadratic performance index function is

$$E(k) = \frac{1}{2}\sum_{i=1}^{k} e^2{}_\lambda(i) \tag{8}$$

In order to make modification of weighted coefficient $w_{i=1,2,3}$ decrease along the reduce direction of $E(t)$, and (9) can be concluded.

$$\begin{aligned} \Delta w_i &= w_i(k) - w_i(k-1) = -\eta \partial E(k) / \partial w_i(k) \\ &= \eta e_2(k) x_i(k) \partial \hat{\lambda}_s(k) / \partial u_i(k) \end{aligned} \quad (i=1, 2, 3) \tag{9}$$

Learning algorithm is as follows

$$u(k) = u(k-1) + K\sum_{i=1}^{3}(x_i(k) w_i(k)) / \sum_{i=1}^{3} |w_i(k)| \tag{10}$$

Where, K is neuron proportional coefficient, $w_{i=1,2,3}$ is the weighting efficient of $x_{i=1,2,3}$, $0 < w_{i=1,2,3} < U_{\max}$, and $U_{\max}$ is maximum amplitude.

Single neuron weighting efficient can be expressed

$$\begin{cases} w_1(k+1) = w_1(k) + \eta_P(k) e_\lambda(k) x_1(k) \operatorname{sgn}(\partial \hat{\lambda}_s(k) / \partial u_1(k)) \\ w_2(k+1) = w_2(k) + \eta_I(k) e_\lambda(k) x_2(k) \operatorname{sgn}(\partial \hat{\lambda}_s(k) / \partial u_2(k)) \\ w_3(k+1) = w_3(k) + \eta_D(k) e_\lambda(k) x_3(k) \operatorname{sgn}(\partial \hat{\lambda}_s(k) / \partial u_3(k)) \end{cases} \tag{11}$$

where, η_p, η_I, and η_D are proportional, integral and differential weights of learning rate, respectively.

PID parameters are

$$\begin{cases} k_{P\lambda} = K w_1(k) / |w_1(k)| \\ k_{I\lambda} = K w_2(k) / |w_2(k)| \\ k_{D\lambda} = K w_3(k) / |w_3(k)| \end{cases} \tag{12}$$

5. Stability Analysis and Parameter Selection

5.1 Lyapunov stability analysis

Define a Lyapunov candidate function

$$v(k) = \frac{1}{2}\sum_{i=1}^{k} e^2(i) > 0 \tag{13}$$

In the learning process, the change of $v(t)$ can be expressed as follows

$$\Delta v(k) = \frac{1}{2}\sum_{i=0}^{k}[e^2(i+1) - e^2(i)] \tag{14}$$

Assuming $e(0) = 0$, (15) can be concluded.

$$\Delta v(k) = \frac{1}{2}\sum_{i=0}^{k}\{[e(i) + \Delta e(i)]^2 - e^2(i)\} \tag{15}$$

The change of $v(t)$ can also be expressed as follows

$$\begin{aligned} e(k+1) &= e(k) + [\partial e(k) / \partial w(k)]^T \times \Delta w(k) \\ &= e(k) + \Delta e(k) \end{aligned} \tag{16}$$

Assuming

$H = [\partial e(k) / \partial w(k)]^T = (\partial e(k) / \partial w(k))[\partial u(k) / \partial w(k)]^T$, (17) can be concluded.

$$\Delta e(k) = -\eta H H^T e(k) \tag{17}$$

Substituting (17) in (15) yields

$$\Delta v(k) = -\frac{1}{2}\sum_{i=0}^{k}(H^T e(i))^T [2\eta - \eta^2 H H^T](H^T e(i)) \tag{18}$$

For global asymptotic stability, $\Delta v(k) < 0$. Hence, the following equations can be deduced:

$$2\eta - \eta^2 H H^T > 0 \tag{19}$$

So, the scope of the learning rate is

$$0 < \eta < 2(H H^T)^{-1} \tag{20}$$

For $\Delta v(k) < 0$, (21) can be concluded from (14)

$$\lim_{k\to\infty} e(k) = 0 \tag{21}$$

So learning algorithm is convergence, and control system is stability.

5.2 Parameter selection

When the error is large, proportional coefficient *K* should large for having fast start-up speed. And when the error is small, *K* should small for preventing overshoot. Generally, nonlinear adjustment formula for K is shown in (20) [20].

$$K(k) = k_0 + A(i_s(k) - \hat{i}_s(k))^3 / i_s(k)^2 \tag{22}$$

Where k_0 is steady-state proportional coefficient, *A* is regulation coefficient.

But a critical problem of the low-speed operation of the flux observer is the dc-measurement offset. In reality, v_α and v_β are reconstructed from the dc-bus voltage Vdc and the switching status. Any dc-measurement error, switch voltage, and dead-time voltage are reflected in both v_α and v_β, especially in low-speed performance. In Fig. 9, torque and flux estimation error curves are provided under given speed 1500rpm and 3Nm load conditions. In Fig. 9(a), it is obvious that the operational performance of control system is poor.

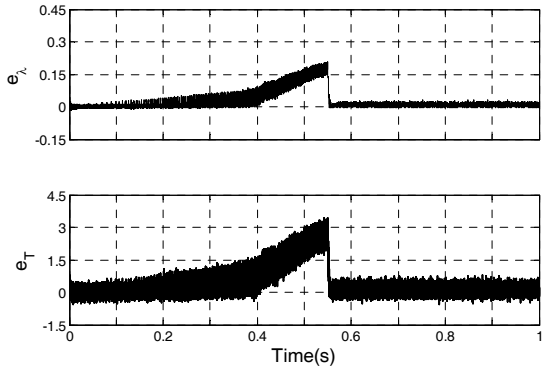

(a) Before compensation

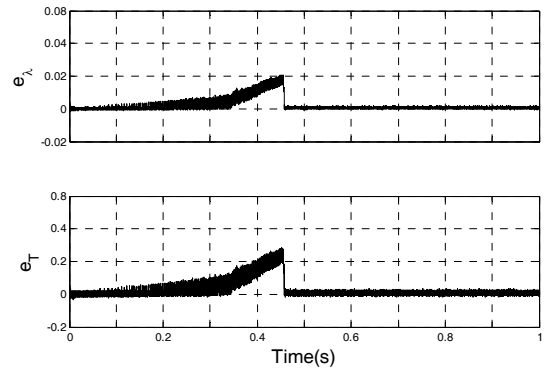

(b) After compensation

Fig. 9. Torque and flux estimation error

The effects of the dc offset can be alleviated by introducing a variable PI component in regulation coefficient as follows:

$$k(k) = k_0 + A[\frac{\omega_{r\max} - \omega_r}{\omega_{r\max}}(k_p e(k) + k_i \sum_{i=0}^{k} e(i)) + 1] \times (i_{s\alpha}(k) - \hat{i}_{s\alpha}(k))^3 / i_{s\alpha}(k)^2 \tag{23}$$

Where $k_p = R_s / L_s$, and $k_i = 1/L_s$. $A \approx k_0/10$ is practical for a real drive.

The advantages of (23) is the function of last item can be obviously increased, when the error is large at the beginning operation or flux error is large, especially at low-speed. With the increasing of speed or flux error becoming small, the function of last item is obviously weakened, and the overshoot is limited. After compensation, the result is shown in Fig. 9(b).

6. Simulation and Experiment Results

According to above analysis, it can get the expressions of rotor position, speed and electromagnetic torque as follows.

$$\hat{\theta}_r = \tan^{-1}((\hat{\lambda}_{s\beta} - L_s i_{s\beta})/(\hat{\lambda}_{s\alpha} - L_s i_{s\alpha})) \tag{24}$$

$$\hat{\omega}_r = d\hat{\theta}_r / dt \tag{25}$$

$$\hat{T}_e = \frac{3P}{2}[\hat{\lambda}_{s\alpha} i_{s\beta} - \hat{\lambda}_{s\beta} i_{s\alpha}] \tag{26}$$

Direct torque control system structure of BLDCM is shown in Fig. 7. Based on Fig. 7, simulation model has been built using Matlab/Simulink, and parameters of BLDCM are shown in Table 4. Simulation results are shown in Fig. 10.

Fig. 10 describes the simulation results which is control system starts up with 5Nm load, and load sudden drops from 5Nm to 1Nm. From Fig. 10(a), it can be seen flux observation curve is smooth, and good observation effect of flux can provide accurate information for system control. In Fig. 10(b) and (e), current curve of DTC is smoother than that of DCC, and DTC can improve the current distortion causing by uncontrolled phase. In Fig. 10(c), (d), (f), and (g), it is shown that the DTC can effectively alleviate commutation torque ripple, and improve the torque and speed response.

Table 4. Parameter of BLDCM

Rated voltage	V	310V	Stator induction	L	5.22mH
Rated torque	Te	5Nm	rotational inertia	J	0.08kg·m^2
Rated speed	n	1500	number of pole pairs	Pn	2
Stator resistance	Rs	1.5Ω			

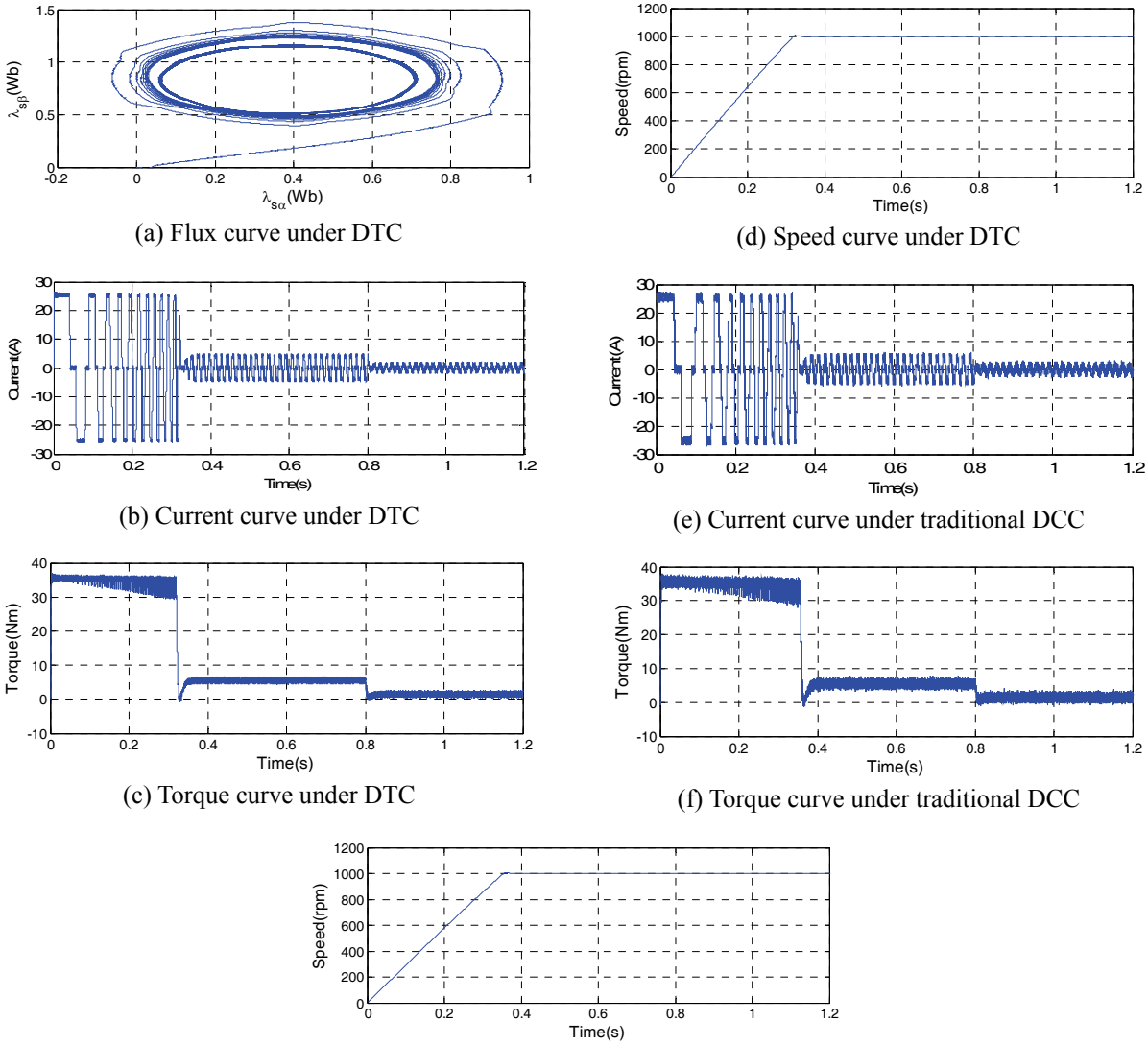

(a) Flux curve under DTC

(d) Speed curve under DTC

(b) Current curve under DTC

(e) Current curve under traditional DCC

(c) Torque curve under DTC

(f) Torque curve under traditional DCC

(g) Speed curve under traditional DCC

Fig. 10. Simulation curve

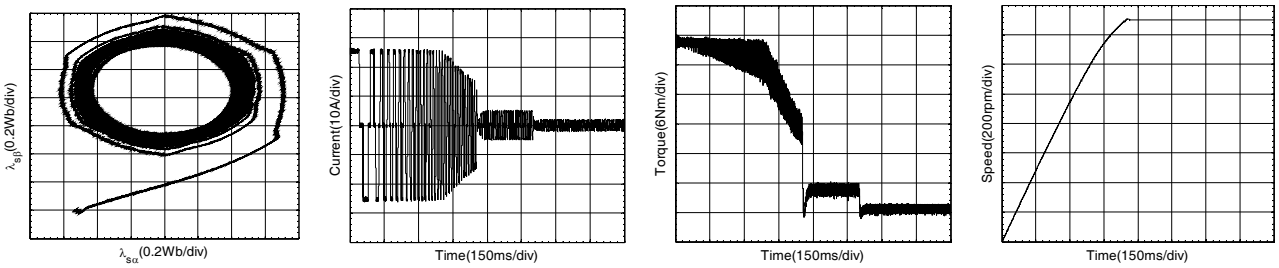

(a) Flux curve (b) Current curve (c) Torque curve (d) Speed curve

Fig. 11. Experimental curves for DTC under high speed

Based on the above research content, BLDCM control system has been established with IPM (Intelligent Power Module) devices, and dsPIC6010A is used as main controller. Experimental results are shown in Fig. 11 and 12 under torque changed from 5Nm to 1Nm at high speed (1500rpm) and low speed (15rpm). Fig. 13 shows the experimental results under traditional DCC, when torque is changed from 5Nm to 1Nm at high speed (1500rpm) and low speed (15rpm).

In Fig. 11(a) and Fig. 12(a), since the dc voltage compensation has been introduced, flux observation precision has been improved and it can provide accurate flux size

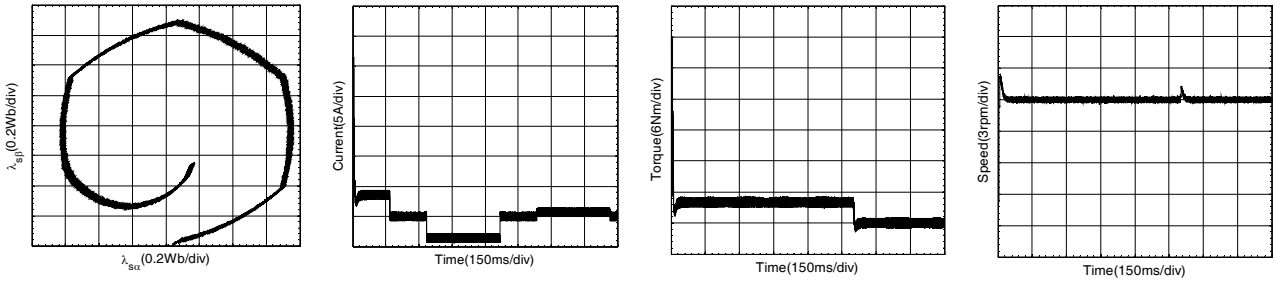

(a) Flux curve (b) Current curve (c) Torque curve (d) Speed curve

Fig. 12. Experimental curves for DTC under low speed

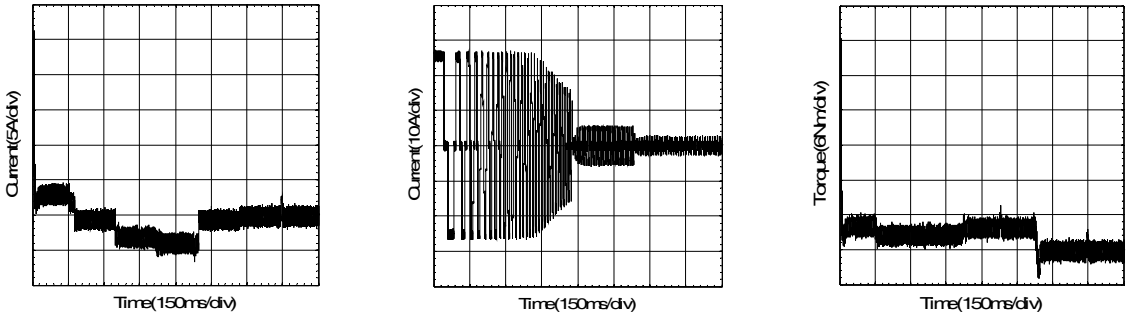

(a) Current for low speed (b) Current for high speed (c) Torque for low speed

(d) Torque for high speed (e) Speed for low speed (f) Speed for high speed

Fig. 13. Experimental curves for traditional DCC

and position information for the DTC.

From Fig. 11(b), Fig. 12(b) and Fig. 13(a, b), it can be seen that the DTC can improve current distortion causing by uncontrolled phase, and the current response speed is faster than that of traditional DCC.

From Fig. 11(c, d), Fig. 12(c, d) and Fig. 13(c, d, e, f), it can be seen that the DTC can improve torque pulsation, and the DTC has better dynamic and static performance characteristics of torque and speed than that of traditional DCC.

7. Conclusion

In this paper, a novel voltage space vector modulation scheme, an optimal switching table and a single neuron stator flux observer for direct torque control were proposed. The flux observer does not require speed adaptation and is not susceptible to speed estimation errors, especially, at low speed. The stability of the proposed observer is proven by the Lyapunov stability analysis. The effects of dc-measurement offsets are mitigated by incorporating an integral compensating term in the observer gain. The proposed single neuron flux observer is capable of delivering high performance over a wide speed range, including very low speeds. As a consequence, current distortion and torque pulsation are effectively improved, and the response speed of speed and torque are significantly improved. The proposed DTC can also be used in servo control for BLDCM.

Acknowledgements

This work was supported by Universities Science and Technology Fund Planning Project of Tianjin (20130419);

National science and technology support plan (2013 BAJ09B03).

References

[1] K.-W. Lee, D.-K. Kim, B.-T. Kim, et al, "A novel starting method of the surface permanent-magnet BLDC motors without position sensor for reciprocating compressor," IEEE Trans. Ind. Appl., vol. 44, no. 1, pp. 85-92, Feb. 2008.

[2] D.-K. Kim, K.-W. Lee, B.-I. Kwon, "Commutation torque ripple reduction in a position sensorless brushless DC motor drive," IEEE Trans. Power Electron., vol. 21, no. 6, pp. 1762-1768, Nov. 2006.

[3] B.-K. Lee, T.-H. Kim, and M. Ehsani, "On the feasibility of four-switch three-phase BLDC motor drives for low cost commercial applications: Topology and control," IEEE Trans. Power Electron., vol. 18, no. 1, pp. 164-172, Jan. 2003.

[4] Joon Ho Lee, Tae Sung Kim, and Dong Seok Hyun, "A study for improved of speed response characteristic in four-switch three-phase BLDC motor," in Proc. IEEE Ind. Electron. Soc. Conf., 2004, vol. 2, pp. 1339-1343.

[5] A. H. Niasar, H. Moghbeli, A. Vahedi, "Adaptive neuron-fuzzy control with fuzzy supervisory learning algorithm for speed regulation of 4-switch inverter brushless DC machines," in Proc. IEEE Power Electron. Motion Control Conf., 2006, pp. 1-5.

[6] A.H. Niassar, A. Vahedi, and H. Moghbelli, "Analysis and control of commutation torque ripple in four-switch three-phase brushless DC motor drive," in Proc. IEEE Ind. Technol. Conf., 2006, pp. 239-246.

[7] Salih Baris Ozturk, William C. Alexander, Hamid A. Toliyat, "Direct Torque Control of Four-Switch Brushless DC Motor with Non-sinusoidal Back-EMF", IEEE Transactions on Power Electronics, Vol. 25, no. 2, pp. 263-271, Feb. 2010.

[8] J. Kim, J. Hong, and K. Nam, "A current distortion compensation scheme for four-switch converters," IEEE Trans. Power Electron., vol. 24, no. 4, pp. 1032-1040, Apr. 2009.

[9] P.P. Acarnley and J.F. Watson, "Review of position-sensorless operation of brushless permanent-magnet machines," IEEE Trans. Ind. Electron., vol. 53, no. 2, pp. 352-362, Apr. 2006.

[10] M.B. de Rossiter Corrêa, C.B. Jacobina, E.R.C. da Silva, and A. M. N. Lim, "A general PWM strategy for four-switch three-phase inverters," IEEE Trans. Power Electron., vol. 21, no. 6, pp. 1618-1627, Nov. 2006.

[11] C.-T. Lin, C.-W. Hung, and C.-W. Liu, "Position sensorless control for four-switch three-phase brushless DC motor drives," IEEE Trans. Power Electron., vol. 23, no. 1, pp. 438-444, Jan. 2008.

[12] C. Xia, Z. Li, and T. Shi, "A control strategy for four-switch three phase brushless dc motor using single current sensor," IEEE Trans. Ind. Electron., vol. 56, no. 6, pp. 2058-2066, Jun. 2009.

[13] Q. Fu, and H. Lin, "Sliding Mode Driving Strategy for Four-switch Three-phase Brushless DC Motor," SICE-ICASE, 2006. International Joint Conference, 2006, pp. 696-701.

[14] Z. Q. Zhu, K. Utaikaifa, K. Hoang, Y. Liu, and D. Howe, "Direct torque control of three-phase PM brushless AC motor with one phase open circuit fault," in Proc. IEEE Int. Conf. Elect. Mach. Drives, May 3-6, 2009, pp. 1408-1415.

[15] Q. Fu, H. Lin, H. T. Zhang, "Single-current-sensor Sliding Mode Driving Strategy For Four-switch Three-phase Brushless DC Motor," Industrial Technology, 2006. ICIT 2006. IEEE International Conferences, Dec. 2006, pp. 2396-2401.

[16] C. Tsung Lin, C. Wen Hung, C. Wen Liu, "Sensorless Control for Four-Switch Three-Phase Brushless DC Motor Drives", Proceeding of the 2006 IEEE Industry Applications Conference Forty-First IAS Annual Meeting (IAS'06), 2006, vol. 4, pp. 2049-2053.

[17] A. Halvaei Niasar, H. Moghbeli, A. Vahedi, "Sensorless Control for Four-Switch, Three-Phase Brushless DC Motor Drive", Proceeding of the 15'th Iranian Conference on Electrical Engineering, 2007, vol. 1, pp. 2048- 2053.

[18] Abolfazl Halvaei Niasar, Abolfazl Vahedi, Hassan Moghbelli, "A Novel Position Sensorless Control of a Four-Switch, Brushless DC Motor Drive Without Phase Shifter", IEEE Transactions on Power Electronics, vol. 23, no. 6, pp.3079-3087, NOV. 2008.

[19] G. J. Su, W. McKeever, "Low-cost sensorless control of brushless DC motors with improved speed range," IEEE Trans. Power Electron., vol. 19, no. 2, pp. 296-302, Mar. 2004.

[20] Wang Maoli, Cheng Guanghe, Kong Xiangxin, "A Single Neuron Self-Adaptive PID Controller of Brushless DC Motor," 2011 Third International Conference on Measuring Technology and Mechatronics Automation, 2011, vol. 1, pp. 262- 266.

Lei Pan He received the Ph.D. degrees from HeBei University of Technology, Tianjin, China, in 2014. He is currently a lecturer of Tianjin Chengjian University. His research interests are power converters and motor drives.

Beibei Wang He received Bachelor and Master degree of Engineering in electrical engineering and power electronics from Liaoning Technical University, Liaoning, China in 2006 and 2009 respectively. He is currently a lecturer of Tianjin Chengjian University. His research interests include power converter system and electrical motor drives.

Gang Su He received the Ph.D. degrees from Nankai University, Tianjin, China, in 2005. He is currently a professor of Tianjin Chengjian University. His research interests are control of power converters and motor drives.

Baohua Cheng He received the Ph.D. from Tianjin University, Tianjin, China, in 2014. He is currently a lecturer of Tianjin Chengjian University. His research interests are active power filter and refrigeration system energy saving technology.

Guili Peng He received the Master degrees from Southwest University of Science and Technology, Mianyang, Sichuan, China, in 2007. He is currently a lecturer of Tianjin Chenjian University. His research interests are automatic control theory and Electrical and electronic technology.